Evolution mapping: a new approach to describe matter clustering in the non-linear regime

Ariel G. Sánchez,[1,2]⋆ Andrés N. Ruiz,[3,4] Jenny Gonzalez Jara,[5,6] and Nelson D. Padilla[3]

[1]*Max-Planck-Institut für extraterrestrische Physik, Postfach 1312, Giessenbachstr., 85748 Garching, Germany*
[2]*Universitäs-Sternwarte Müchen, Fakultät für Physik, Ludwig- Maximilians-Universität München, Scheinerstrasse 1, 81679 Müchen, Germany*
[3]*Instituto de Astronomía Teórica y Experimental (CONICET-UNC), Laprida 854, X5000BGR, Córdoba, Argentina*
[4]*Observatorio Astronómico, Universidad Nacional de Córdoba, Laprida 854, X5000BGR, Córdoba, Argentina*
[5]*Instituto de Astrofísica, Pontificia Universidad Católica de Chile, Santiago, Chile*
[6]*Centro de Astro-Ingeniería, Pontificia Universidad Católica de Chile, Santiago, Chile*

ABSTRACT

We present a new approach to describe statistics of the non-linear matter density field that exploits a degeneracy in the impact of different cosmological parameters on the linear dimensionless matter power spectrum, $\Delta_{\rm L}^2(k)$. We classify all cosmological parameters into two groups, shape parameters, which determine the shape of $\Delta_{\rm L}^2(k)$, and evolution parameters, which only affect its amplitude at any given redshift. With this definition, the time evolution of $\Delta_{\rm L}^2(k)$ in models with identical shape parameters but different evolution parameters can be mapped from one to the other by relabelling the redshifts that correspond to the same clustering amplitude, which we characterize by the linear mass fluctuation in spheres of radius 12 Mpc, $\sigma_{12}(z)$. We use N-body simulations to show that the same evolution mapping relation gives a good description of the non-linear power spectrum, the halo mass function, or the full density field. The deviations from the exact degeneracy are the result of the different structure formation histories experienced by each model to reach the same clustering amplitude and can be accurately described in terms of differences in the suppression factor $g(a) = D(a)/a$. These relations can be used to drastically reduce the number of parameters required to describe the cosmology dependence of the power spectrum. We show how this can help to speed up the inference of parameter constraints from cosmological observations. We also present a new design of an emulator of the non-linear power spectrum whose predictions can be adapted to an arbitrary choice of evolution parameters and redshift.

Key words: cosmology: theory – large-scale structure of Universe — methods: statistical — methods: numerical

1 INTRODUCTION

The dramatic progress in the accuracy of cosmological observations in the last decades has marked the start of a data-rich era in cosmology. These data have cemented a new cosmological paradigm, the so-called ΛCDM model (Riess et al. 1998; Perlmutter et al. 1999; Eisenstein et al. 2005; Anderson et al. 2012; Alam et al. 2017; Planck Collaboration et al. 2020; Alam et al. 2021). Based on general relativity, this model is characterized by the presence of two components, dark matter and dark energy, whose nature remains elusive. The quest for deviations from this remarkable picture of the Universe will be the main objective of observational cosmology in the coming years.

The analysis of the large-scale structure (LSS) of the Universe using data from galaxy surveys is one of the most effective routes to challenge the validity of the ΛCDM paradigm. Anisotropic clustering measurements inferred from present-day galaxy redshift surveys such as the Baryon Oscillation Spectroscopic Survey (BOSS, Dawson et al. 2013) or the extended Baryon Oscillation Spectroscopic Survey (eBOSS, Dawson et al. 2016) have been used to map the

expansion and growth of structure histories of the Universe over a wide range of cosmic time (e.g. Alam et al. 2017; Alam et al. 2021). Imaging surveys with precise galaxy shape measurements offer an alternative probe of the LSS of the Universe. The analysis of the distortions of those shapes by the gravitational lensing effect caused by the foreground matter distribution has become a robust cosmological probe (Troxel et al. 2018; Hildebrandt et al. 2018; Hikage et al. 2019; Heymans et al. 2021; DES Collaboration et al. 2021). Galaxy clustering and weak lensing statistics are highly complementary. Their joint analysis breaks the degeneracies between cosmological parameters shown by each probe, resulting in improved cosmological constraints and allows for new tests that are impossible when these data sets are considered separately.

The amount of data from galaxy surveys will increase by orders of magnitude over the next decade. Future surveys like the Dark Energy Spectroscopic Instrument (DESI, DESI Collaboration et al. 2016), the ESA space mission *Euclid* (Laureijs et al. 2011), NASA's Roman Space Telescope (Spergel et al. 2015), or the Legacy Survey of Space and Time (LSST) at the Rubin Observatory (Ivezić et al. 2019), are examples of a new generation of galaxy redshift and imaging surveys that will provide more accurate measurements of the LSS of the

⋆ E-mail: arielsan@mpe.mpg.de

Universe than ever before. The small statistical uncertainties that are expected from these data sets impose demanding constraints on the accuracy of the theoretical models that will be used to describe them.

A basic ingredient of the analysis of LSS data sets is the modelling of the matter power spectrum, $P(k)$. Galaxy clustering analyses have largely followed perturbation-theory based models (e.g. Sánchez et al. 2017; Grieb et al. 2017; Tröster et al. 2020; d'Amico et al. 2020; Ivanov et al. 2020). Although this approach has proven to be an efficient way to obtain fast an accurate theoretical predictions, its applicability is limited to scales in the mildly non-linear regime. Studies including weak lensing measurements, which have been based on small scales where non-linearities are strong, have mostly relied on fitting functions based on numerical simulations such as HALOFIT (Smith et al. 2003; Takahashi et al. 2012; Bird et al. 2012) or the halo model (Mead et al. 2015, 2016, 2021). However, the accuracy of these recipes might not be enough for future surveys.

The analysis of the upcoming samples will require a consistent theoretical framework to describe galaxy clustering and weak lensing statistics that is accurate over a wide range of scales, including the deeply non-linear regime. High-resolution numerical simulations would be an ideal tool to help construct such models. As the response of the non-linear power spectrum to changes in the cosmological parameters is smooth, it is possible to build accurate interpolation schemes or emulators, calibrated on a relatively small number of simulations (Heitmann et al. 2010, 2016; DeRose et al. 2018; Garrison et al. 2018; Euclid Collaboration et al. 2018, 2020; Angulo et al. 2021). This technique can also be applied to additional statistics of the density field such as, e.g., the halo mass function (Heitmann et al. 2016; McClintock et al. 2019; Bocquet et al. 2020), opening up the possibility to perform a battery of cosmological tests based on a consistent theoretical description. However, emulators are limited by the parameter space and redshifts sampled during their calibration process. Currently available emulators only sample a few cosmological parameters, often within restrictive ranges, and are not applicable to more general parameter spaces.

In this paper, we present a new approach to construct general models of statistics of the non-linear matter density field that are not restricted to a given parameter space or redshift range. Our method, to which we refer as evolution mapping, is based on the fact that the non-linear evolution of the density field is primarily driven by the linear dimensionless matter power spectrum, $\Delta_L^2(k) = k^3 P_L(k)/2\pi^2$ (Hamilton et al. 1991; Peacock & Dodds 1994; Ma & Fry 2000). This means that the degeneracies between different cosmological parameters with respect to their impact on $\Delta_L^2(k)$ will also be approximately inherited by its non-linear counterpart. Therefore, the use of a parameter basis that makes such degeneracies more evident can be exploited to simplify the description of the non-linear $\Delta^2(k)$. With this in mind, we divide all cosmological parameters into two groups, shape parameters, which determine the shape of $\Delta_L^2(k)$, and evolution parameters, which only control its amplitude at a given redshift z. We build upon the results of Sánchez (2020), who studied the problems caused by the common practice of expressing theoretical predictions of cosmological measurements in units of h^{-1}Mpc. Sánchez (2020) showed that, when the power spectrum is expressed in Mpc units, parameters like the amplitude of the scalar mode, A_s, and the dimensionless Hubble constant, h, follow a perfect degeneracy that defines the amplitude of $P_L(k)$. As we discuss later on, this is just a particular example of a much broader degeneracy involving all evolution parameters. We propose to exploit this degeneracy to describe the non-linear density field in terms of a reduced number of parameters.

The structure of this paper is as follows: in Sec. 2 we present our

classification of cosmological parameters into shape and evolution parameters. In Sec. 3, we describe the evolution-mapping degeneracy followed by all evolution parameters and use numerical simulations to show that this relation, which is exact in linear theory, is also approximately inherited by the non-linear density field. In Sec. 4 we discuss a few practical applications of evolution mapping to simplify the analysis and modelling of cosmological observables. Finally, Sec. 5 presents our main conclusions. Throughout this paper, all scales are assumed to be in Mpc units and masses are expressed in $M_\odot$ without introducing any factors of h.

2   COSMOLOGICAL PARAMETERS AND THEIR IMPACT ON THE MATTER POWER SPECTRUM

The matter power spectrum depends on a large number of cosmological parameters describing the homogeneous background model and the properties of the primordial density fluctuations. Although different parametrisations are in principle equivalent, the modelling of the non-linear power spectrum can be significantly simplified when studied in a parameter basis in which the degeneracies at the linear level become more explicit.

We will describe the background model in terms of the physical density parameters

$$\omega_i := \frac{8\pi G}{3\,H_{100}^2}\rho_i, \tag{1}$$

where ρ_i represents the present-day density of each energy component i (e.g. baryons, cold dark matter, dark energy, etc.), and H_{100} is a constant given by

$$H_{100} := 100\,\mathrm{km\,s^{-1}\,Mpc^{-1}}, \tag{2}$$

which is introduced for historical reasons and ensures that the resulting physical density parameters are dimensionless. The properties of each energy component can be described by their corresponding equation of state parameters

$$w_i := \frac{p_i}{\rho_i c^2}, \tag{3}$$

specifying the relation between their density and pressure, which can be time dependent. The complete characterization of the background homogeneous model requires to specify its spatial curvature, K, which can be expressed also as a physical curvature density parameter defined as

$$\omega_K := -\frac{Kc^2}{H_{100}^2}. \tag{4}$$

The standard ΛCDM model corresponds to a flat Universe (i.e., $\omega_K = 0$) containing contributions from photons, baryons, cold dark matter, neutrinos, and dark energy, which behaves analogously to a cosmological constant with an equation of state parameter $w_{\mathrm{DE}} = -1$.

Besides describing the homogeneous background evolution of the Universe, the full characterization of a cosmological model requires parameters that describe its inhomogeneities. The primordial density fluctuations generated by inflation are commonly characterized in terms of the amplitude, A_s, and the spectral index, n_s, of the scalar mode at the pivot scale $k_p = 0.05\,\mathrm{Mpc^{-1}}$. This list is not exhaustive, as it could include additional parameters such as, e.g., the running of the scalar spectral index α_s.

Multiple equivalent parameter bases could be used to specify a given cosmological model. For example, it is common to replace

one of the physical density parameters (e.g. ω_{DE}) by the dimensionless Hubble parameter, h, which is given by the sum of all energy contributions as

$$h^2 := \sum_i \omega_i, \qquad (5)$$

and defines the present-day value of the Hubble parameter as $H_0 = h H_{100}$. The contributions of the various energy components can also be characterized in terms of the density parameters

$$\Omega_i := \omega_i / h^2. \qquad (6)$$

We will refer to the parameters Ω_i as the *fractional* density parameters, as they represent the fraction of the total energy density of the Universe corresponding to component i. The overall amplitude of the power spectrum can be characterized by the RMS linear perturbation theory variance at a reference scale R, given by

$$\sigma^2(R) = \frac{1}{2\pi^2} \int dk\, k^2 P_L(k) W^2(kR), \qquad (7)$$

where $W(kR)$ is the Fourier transform of a top-hat window of radius R. Traditionally, this reference scale has been set to $R = 8\, h^{-1}$ Mpc. We will denote the corresponding value of $\sigma(R)$ as $\sigma_{8/h}$ to emphasize its dependency on the value of h. Sánchez (2020) showed that, due to this dependency, $\sigma_{8/h}$ does not correctly capture the impact of h on $P_L(k)$. This problem can be avoided by describing the amplitude of the matter power spectrum in terms of a reference scale in Mpc. As proposed by Sánchez (2020), a convenient choice is 12 Mpc, which results in a mass variance σ_{12} with a similar value to the standard $\sigma_{8/h}$ for $h \sim 0.67$. Alternatively, instead of $\sigma(R)$ on a given scale, the amplitude of density fluctuations could be characterized directly in terms of the value of the dimensionless power spectrum, $\Delta_L^2(k_p)$, at a reference wavenumber, k_p, in Mpc^{-1} (see, e.g., Pedersen et al. 2021). We will follow Sánchez (2020) and use σ_{12} as it is closer to the most commonly used $\sigma_{8/h}$.

To best exploit the intrinsic degeneracies between different cosmological parameters, we can classify them according to their impact on $\Delta_L^2(k)$, into two groups, *shape* and *evolution* parameters. The first set includes the parameters that define the shape of the primordial power spectrum and the transfer function. Examples of these parameters are

$$\boldsymbol{\Theta}_s = \left(\omega_\gamma, \omega_b, \omega_c, n_s, \cdots \right), \qquad (8)$$

that is, the physical densities of radiation, baryons, cold dark matter and neutrinos, and the scalar spectral index. Once the values of the parameters $\boldsymbol{\Theta}_s$ are specified, the shape of the linear-theory dimensionless matter power spectrum is completely defined. At the linear level, all other parameters only affect the amplitude of $\Delta_L^2(k)$ at any given redshift. These evolution parameters include

$$\boldsymbol{\Theta}_e = (A_s, \omega_K, \omega_{DE}, w_{DE}(a), \cdots). \qquad (9)$$

These are the amplitude of the primordial scalar power spectrum, the curvature and dark energy density parameters and the dark energy equation of state parameter, including all possible parametrizations of its time evolution, such as the standard linear parametrization of Chevallier & Polarski (2001) and Linder (2003)

$$w_{DE}(a) = w_0 + w_a (1 - a). \qquad (10)$$

Alternatively, in early dark energy (EDE) models, which are characterized by a fractional dark energy density parameter that asymptotes to a value $\Omega_{DE,e}$ at very high redshift, the time evolution of $w_{DE}(a)$ can be parametrized as (Wetterich 2004)

$$w_{DE}(a) = \frac{w_0}{(1 - b \ln(a))^2}, \qquad (11)$$

Table 1. Parameters of our reference flat ΛCDM model.

Parameter	value
ω_b	0.02244
ω_c	0.1206
ω_ν	0
n_s	0.96
ω_K	0
ω_{DE}	0.3059
w_{DE}	-1
h	0.67

where

$$b = \frac{3w_0}{\ln\left(\frac{1 - \Omega_{DE,e}}{\Omega_{DE,e}}\right) + \ln\left(\frac{1 - \Omega_m}{\Omega_m}\right)}. \qquad (12)$$

The physical density of massive neutrinos, ω_ν, deserves a special mention. In models with massive neutrinos, the growth factor becomes scale-dependent even at the lineal level. Therefore, ω_ν cannot be strictly classified as a shape or evolution parameter. We will focus on cosmologies with $\omega_\nu = 0$ and leave the discussion on how this parameter can be included in the formalism presented here for a forthcoming analysis.

Present-day measurements of the cosmic microwave background (CMB) alone can accurately constrain the values of most of the shape parameters. However, they only provide weak constraints on the evolution parameters for general cosmologies. The inverse is true for LSS measurements. When analysed independently of other data sets, LSS data can only provide weak constraints on the values of the shape parameters. However, if the shape parameters are constrained by an independent data set, LSS data can provide precise measurements of the evolution parameters. This difference makes CMB and LSS highly complementary cosmological probes and one of our most powerful routes to obtain accurate and robust cosmological constraints.

3 EVOLUTION MAPPING

3.1 Linear evolution of density perturbations

As evolution parameters only change the amplitude of $\Delta_L^2(k|z)$, their effect follows a perfect degeneracy. Once a given set of shape parameters $\boldsymbol{\Theta}_s$ has been specified, the power spectra of all the models defined by different choices of the evolution parameters $\boldsymbol{\Theta}_e$ and z that lead to the same clustering amplitude are identical. This degeneracy can be described by the value of $\sigma_{12}(z)$ as

$$\Delta_L^2(k|z, \boldsymbol{\Theta}_s, \boldsymbol{\Theta}_e) = \Delta_L^2\left(k|\boldsymbol{\Theta}_s, \sigma_{12}(z, \boldsymbol{\Theta}_s, \boldsymbol{\Theta}_e)\right). \qquad (13)$$

At the linear level, the time evolution of $\Delta_L^2(k)$ in models characterized by the same values of the shape parameters $\boldsymbol{\Theta}_s$ but different choices of $\boldsymbol{\Theta}_e$ can be mapped from one to the other simply by relabelling the redshifts that correspond to the same values of σ_{12}. We will therefore refer to equation (13) as the evolution mapping relation for the power spectrum.

Note that the relation of equation (13) is also applicable to $P_L(k)$ when it is expressed in Mpc instead of the traditional h^{-1}Mpc. This degeneracy is also lost when the amplitude of $P_L(k)$ is described in terms of $\sigma_{8/h}$, which depends on the particular value of h. The fractional density parameters Ω_i of equation (6) also obscure this degeneracy as they represent a mixture of shape and evolution parameters.

Table 2. Test cosmologies considered in this analysis and used to define the Aletheia simulations described in Sec. 3.2. All models are characterized by identical shape parameters as in the reference cosmology defined in Table 1 and different evolution parameters. Model 0 corresponds to our reference ΛCDM universe. Models 1 to 7 are defined by changing one parameter of the reference case. Model 8 corresponds to an EDE cosmology. We consider the five reference values of σ_{12} listed in the upper part of the table. For each cosmology, we list the redshifts at which $\sigma_{12}(z)$ matches the reference values given in the upper part of the table, which define the outputs of the Aletheia simulations.

Model	Definition	$\sigma_{12} = 0.343$	$\sigma_{12} = 0.499$	$\sigma_{12} = 0.611$	$\sigma_{12} = 0.703$	$\sigma_{12} = 0.825$
Model 0	Reference ΛCDM as in Table 1.	2.000	1.000	0.570	0.300	0.00
Model 1	ΛCDM, $\omega_{DE} = 0.2874$ ($h = 0.55$).	1.761	0.859	0.480	0.248	0.00
Model 2	ΛCDM, $\omega_{DE} = 0.6090$ ($h = 0.79$).	2.231	1.137	0.659	0.352	0.00
Model 3	wCDM, $w_{DE} = -0.85$.	2.100	1.044	0.590	0.307	0.00
Model 3	wCDM, $w_{DE} = -1.15$.	1.923	0.964	0.553	0.293	0.00
Model 5	Dynamic dark energy (equation (10)), $w_a = -0.2$.	1.973	0.990	0.566	0.299	0.00
Model 6	Dynamic dark energy (equation (10)), $w_a = 0.2$.	2.031	1.011	0.574	0.301	0.00
Model 7	Non-flat ΛCDM, $\Omega_K = -0.05$.	1.938	0.978	0.561	0.297	0.00
Model 8	EDE model, $w_0 = -1.15$, $\Omega_{DE,e} = 10^{-5}$.	2.020	0.997	0.565	0.297	0.00

Sánchez (2020) discussed the perfect degeneracy between h and A_s for a ΛCDM model, which can be characterized by a constant value of σ_{12}. This is a particular case of the evolution mapping relation of equation (13). For a general cosmology, h is a combination of shape and evolution parameters. However, for a ΛCDM universe, fixing the values of the shape parameters ω_b and ω_c and varying h corresponds to assuming different values of the purely evolution parameter ω_{DE}.

As an illustration of the relation of equation (13), we consider a set of nine cosmological models characterized by the same values of the shape parameters Θ_s and a wide range of evolution parameters Θ_e. To define these test cosmologies, we use as a reference the cosmological parameters specified in Table 1, which correspond to a flat ΛCDM Universe. Table 2 defines these cosmologies, labelled as models 0 to 8, which are specified by changing the value of one parameter of the reference case. While model 0 corresponds to a flat ΛCDM universe close to the best-fitting model to the latest *Planck* data (although with no contribution from massive neutrinos), the remaining cases include different values of h (corresponding to different values of ω_{DE}), a time-independent dark energy equation of state $w_{DE} \neq -1$, dynamical dark energy models with $w_a \neq 0$, a non-flat universe, and an EDE cosmology. The values of A_s of these models were defined to normalize their power spectra to give $\sigma_{12} = 0.825$ at $z = 0$. With the exception of model 0, these models were not chosen to represent viable cosmologies to describe our Universe. They represent extreme cases that deviate significantly from the ranges of the evolution parameters allowed by present-day observations.

The upper panel of Fig. 1 shows the redshift at which these test cosmologies reach a given value of σ_{12}. Equation (13) implies that the linear power spectra of these models will be identical when evaluated at the redshifts that correspond to the same value of σ_{12}. As an illustration of this relation, we used the five values of σ_{12} specified in the upper part of Table 2, which are indicated by vertical grey lines in Fig. 1. The redshifts at which the value of $\sigma_{12}(z)$ for each model matches these reference values are also listed in Table 2. As can be seen in the left panel of Fig. 2, when they are evaluated at these redshifts, the linear-theory power spectra of these models are indistinguishable.

Although we have focused on the dark matter power spectrum in real space, a relation equivalent to equation (13) will also be valid for biased tracers in redshift space. In this case, the power spectrum will depend on the linear bias parameter, $b(z)$, and the logarithmic growth rate $f(z) = d \ln D(z)/d \ln a$, with $D(z)$ the linear growth factor and a the scale factor of the Universe (Kaiser 1987). At the
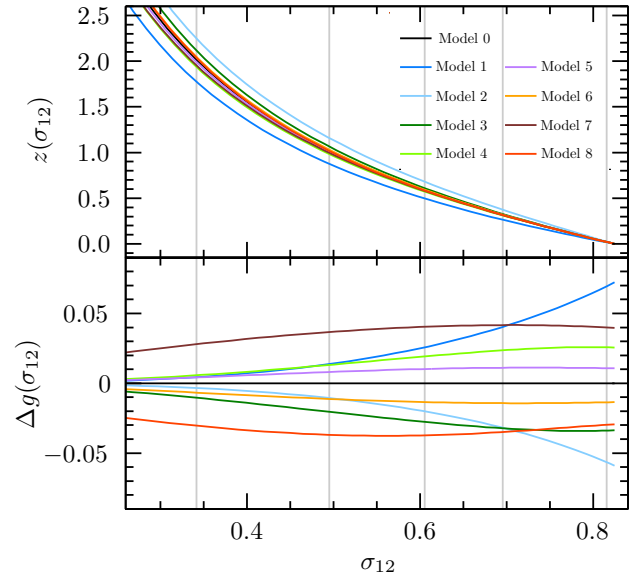

Figure 1. Upper panel: redshift at which the cosmologies defined in Table 2 reach a given value of σ_{12}. Lower panel: the differences in the suppression factors $g(a) = D(a)/a$ between these cosmologies and that of model 0, expressed as a function of σ_{12}. The grey vertical lines in both panels correspond to the five reference values of σ_{12} specified in the upper part of Table 2.

linear level, all models characterized by identical shape parameters and the same values of the parameter combinations $b\sigma_{12}(z)$ and $f\sigma_{12}(z)$ will be identical. For this reason, as discussed by Sánchez (2020), the combination $f\sigma_{12}(z)$ gives a more correct description of the cosmological information content of the pattern of redshift-space distortions than the commonly used $f\sigma_{8/h}(z)$. We leave the analysis of the evolution mapping relation in redshift space and its interplay with the geometric Alcock-Paczynski distortions for future work.

3.2 The non-linear matter power spectrum

It is well known that the non-linear evolution of the matter power spectrum is mainly determined by its linear-theory counterpart $\Delta_L^2(k|z)$ (e.g., Hamilton et al. 1991; Peacock & Dodds 1994, 1996; Jain et al. 1995; Ma & Fry 2000). This fact is at the core of some of the most commonly used tools to account for non-linearities in $P(k)$ (such as, e.g., HALOFIT, Smith et al. 2003), and can be understood in the context of standard perturbation theory (SPT) and other
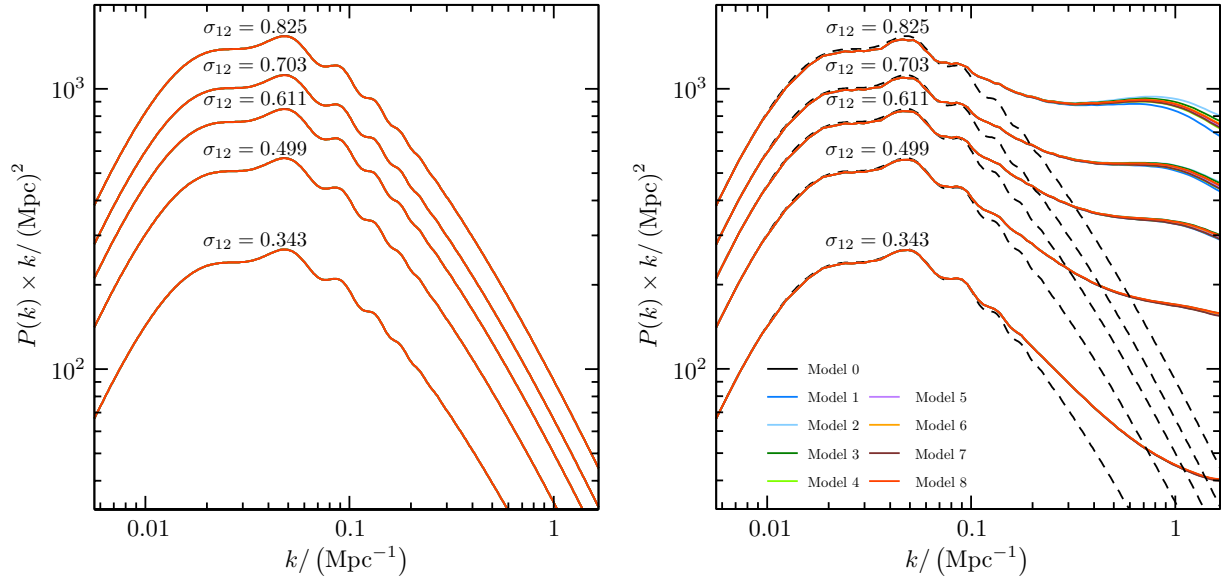
Figure 2. Left panel: linear-theory matter power spectra computed using CAMB (Lewis et al. 2000) of the nine cosmologies defined in Table 2 evaluated at the redshifts at which their values of $\sigma_{12}(z)$ match the reference values indicated by the labels. Following the relation of equation (13), these power spectra are identical. Right panel: matter power spectra of the same models measured from the Aletheia simulations described in Sec. 3.2 (solid lines) compared against their linear-theory predictions (dashed lines). The evolution-mapping relation of equation (13) continues to give a good description of the results.

related approaches. Assuming that the perturbation theory kernels are independent of cosmology, which has been shown to be a good approximation even for non-standard cosmologies (Takahashi 2008; Taruya 2016; Garny & Taule 2021), SPT implies that the non-linear $P(k)$ is a function of the linear power that is independent of the cosmological parameters (Scoccimarro et al. 1998). As an ilustration of this behaviour, we can use renormalized perturbation theory (RPT; Crocce & Scoccimarro 2006), in which the non-linear matter power spectrum, $P(k|z)$, can be written as

$$P(k|z) = P_{\rm L}(k|z)\, G(k|z)^2 + P_{\rm MC}(k|z), \qquad (14)$$

where the propagator $G^2(k|z)$ is obtained by resumming all the terms in the standard perturbation theory expansion that are proportional to the linear power spectrum $P_{\rm L}(k|z)$, and $P_{\rm MC}(k|z)$ contains all mode-coupling contributions. The first term represents the contribution to the final $P(k|z)$ coming from the linearly-evolved power at the same scale k, while the second one describes the contribution from all other scales in the linear power. The propagator is given by a nearly Gaussian damping, whose characteristic scale is defined by an integral over the linear power spectrum. The mode-coupling term can be expressed as a sum of a series of loop contributions, which at N loops involve convolutions over N linear power spectra. Hence, for models with identical $P_{\rm L}(k|z)$, RPT will also lead to the same predictions for the propagator and mode coupling terms, leading to indistinguishable non-linear power spectra. This also applies to other commonly used recipes to describe the non-linear power spectrum that depend exclusively on $P_{\rm L}(k|z)$ (e.g. Taruya et al. 2012; Nishimichi et al. 2017).

Equation (13) provides us with a practical recipe to map the evolution of models characterized by identical shape parameters but different evolution parameters that is exact at the level of linear perturbations. In the context of perturbation theory, the same mapping would be applicable to the power spectrum in the non-linear regime. However, the fundamental assumption of single-stream flow of common perturbation theory approaches eventually breaks down due to shell crossings on small scales. Models with the same $P_{\rm L}(k|z)$ but

different structure growth histories show different non-linear power spectra (Mead 2017). Therefore, there will be deviations from equation (13) in the deeply non-linear regime.

To test this in detail, we ran numerical simulations corresponding to the models listed in Table 2. For each model, we used GADGET-4 (Springel et al. 2021) to generate two simulations following the fixed-paired approach to suppress cosmic variance of Angulo & Pontzen (2016). Each simulation followed the evolution of 1500^3 dark matter particles on a box of side $L_{\rm box} = 1492.5\,{\rm Mpc}$. The simulations were started at redshift $z = 99$ from initial conditions generated with 2LPTIC (Crocce et al. 2006), using the same random phases for all models. Both 2LPTIC and GADGET-4 were modified to include different dark energy models. The Plummer-equivalent softening length was set to $22\,{\rm kpc}$, corresponding to 2 per-cent of the mean inter-particle separation. Each simulation has 5 snapshots chosen to match the redshifts at which each model reaches the reference values of σ_{12} listed in Table 2. We refer to this set as the *Aletheia* simulations.

We computed the matter power spectra of each snapshot of all simulations using the available option in GADGET-4 and averaged the measurements from each pair corresponding to the same model. We focus on wavenumbers $k < 1.5\,{\rm Mpc}^{-1}$ to avoid scales where baryonic effects, which we are ignoring in our analysis, would have to be taken into account. The solid lines in the right panel of Fig. 2 show the resulting power spectra, which exhibit clear deviations from their linear-theory predictions, shown by the black dashed lines. The evolution mapping relation of equation (13) continues to give a very good description of the results. Despite the wide range of evolution parameters covered by these models, their power spectra are in good agreement when they are evaluated at the redshifts that correspond to the same values of σ_{12}.

As expected, unlike the naive expectation based on perturbation theory, the relation of equation (13) is not exact in the deeply non-linear regime. The differences between these models can be seen more clearly in Fig. 3, which shows the ratios of the power spectra of all models with respect to that of model 0. The differences increase with k, and are larger for higher values of σ_{12}. As a reference, the
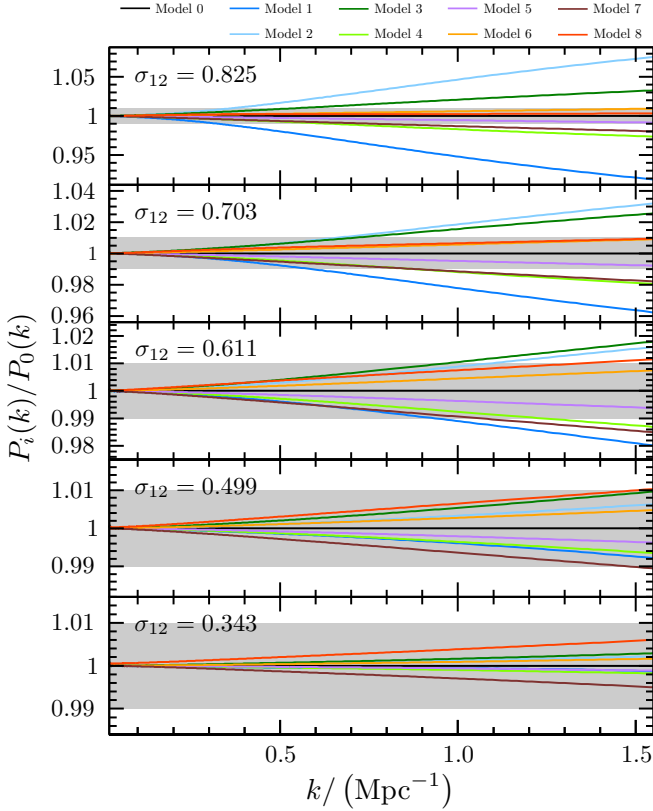
Figure 3. Ratios of the matter power spectra recovered from the different Aletheia simulations and the one corresponding to model 0 for each of our reference values of σ_{12} in different panels.

Figure 4. Ratios of the matter power spectra recovered from model i of the Aletheia simulations and the ones predicted using equation (15) based on the results of model 0 and the differences in the growth of structure histories of these models, characterized by the values of Δg_i and $\Delta g_i'$, for each reference value of σ_{12}.

grey shaded areas shown in all panels correspond to a 1 per-cent difference. These differences with the power spectrum of model 0 remain at the sub-percent level for $\sigma_{12} \leq 0.499$. The maximum differences are seen at $\sigma_{12} = 0.825$, corresponding to $z = 0$ in all models, and can reach an 8 per-cent level at $k = 1.5\,\mathrm{Mpc}^{-1}$. Note also that the models that deviate the most from model 0 are different at each value of σ_{12}. For example, while models 1 and 2 exhibit the most significant deviations for $\sigma_{12} \geq 0.703$, models 7 and 8 show the largest differences for $\sigma_{12} < 0.611$. Despite these differences, the power spectra ratios show no leftover from the signature of baryon acoustic oscillations, indicating that the damping of this signal with respect to the linear-theory prediction is the same in all cosmologies. Appendix A presents a comparison of these results with the predictions of available recipes to model the non-linear $P(k|z)$.

Previous analyses (McDonald et al. 2006; Ma 2007; Mead 2017) have studied the differences in the non-linear power spectrum between cosmological models characterized by the same $P_{\mathrm{L}}(k|z=0)$ but different growth of structure histories. Focusing on ΛCDM cosmologies and models with $w_{\mathrm{DE}} \neq -1$ and identical values of h, these studies have found that their non-linear power spectra at $z = 0$ are also approximately the same in the mildly non-linear regime but differ at smaller scales. Our results extend those findings to general cosmologies characterized by the same shape parameters and any choice of evolution parameters, as long as they are compared at the redshifts at which their values of $\sigma_{12}(z)$ are identical. This is also valid for cosmologies with different values of h as long as the power spectra are expressed in Mpc units.

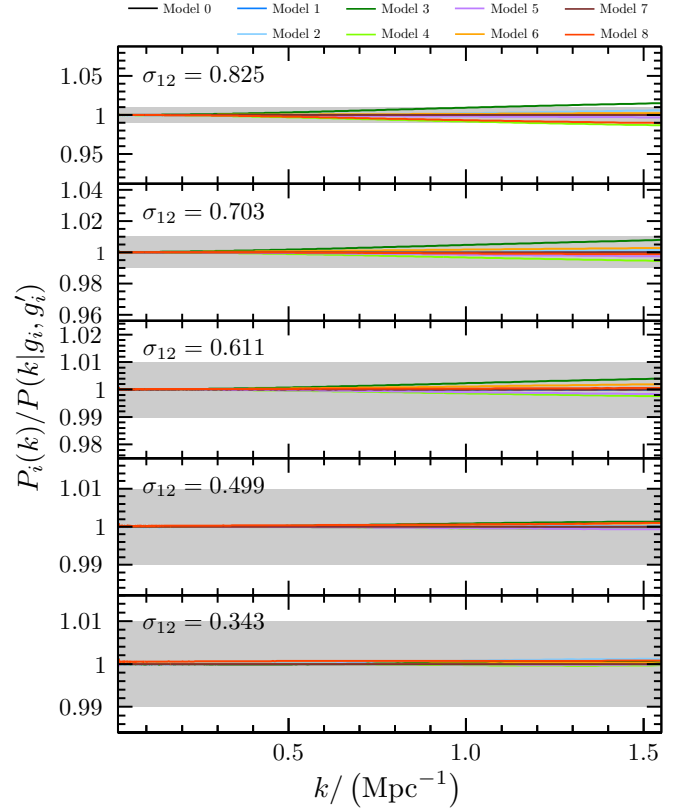Already in the recipe of Peacock & Dodds (1994) the deviations

between the non-linear power spectra of models with identical $\Delta^2_{\mathrm{L}}(k)$ caused by their different structure formation histories are described in terms of the suppression factor $g(a) = D(a)/a$. The lower panel of Fig. 1 shows the differences in the suppression factors $g(a)$ between the different Aletheia cosmologies and that of model 0, expressed as a function of the corresponding value of σ_{12}. These differences show a similar structure to the deviations between the non-linear power spectra shown in Fig. 3. For each of our reference values of σ_{12}, the models with the largest differences $\Delta g(\sigma_{12})$ are the ones for which $P(k)$ exhibits the largest deviations from that of model 0. With this in mind, we tested a simple ansatz to describe the residuals with respect to the evolution mapping relation of equation (13) in terms of $g(\sigma_{12})$ and $g'(\sigma_{12}) = dg(\sigma_{12})/d\sigma_{12}$ as

$$P\left(k|g, g'\right) = P\left(k|g_0, g_0'\right) + \frac{\partial P}{\partial g}\left(k|g_0, g_0'\right)(g - g_0)$$
$$+ \frac{\partial P}{\partial g'}\left(k|g_0, g_0'\right)\left(g' - g_0'\right), \tag{15}$$

where for simplicity we omitted the dependency on Θ_{s} and σ_{12}, which are kept fixed in all terms. To test this ansatz on the Aletheia simulations, we used model 0 as a reference and inferred the derivatives with respect to g and g' using the power spectra of models 1 and 7. We then used these results in equation (15) to compute predictions for the non-linear power spectra of all other models. Fig. (4) shows the ratios of the matter power spectra of all Aletheia simulations and their predictions based on equation (15). By construction, this relation gives a perfect match to the power spectra of models 0, 1, and
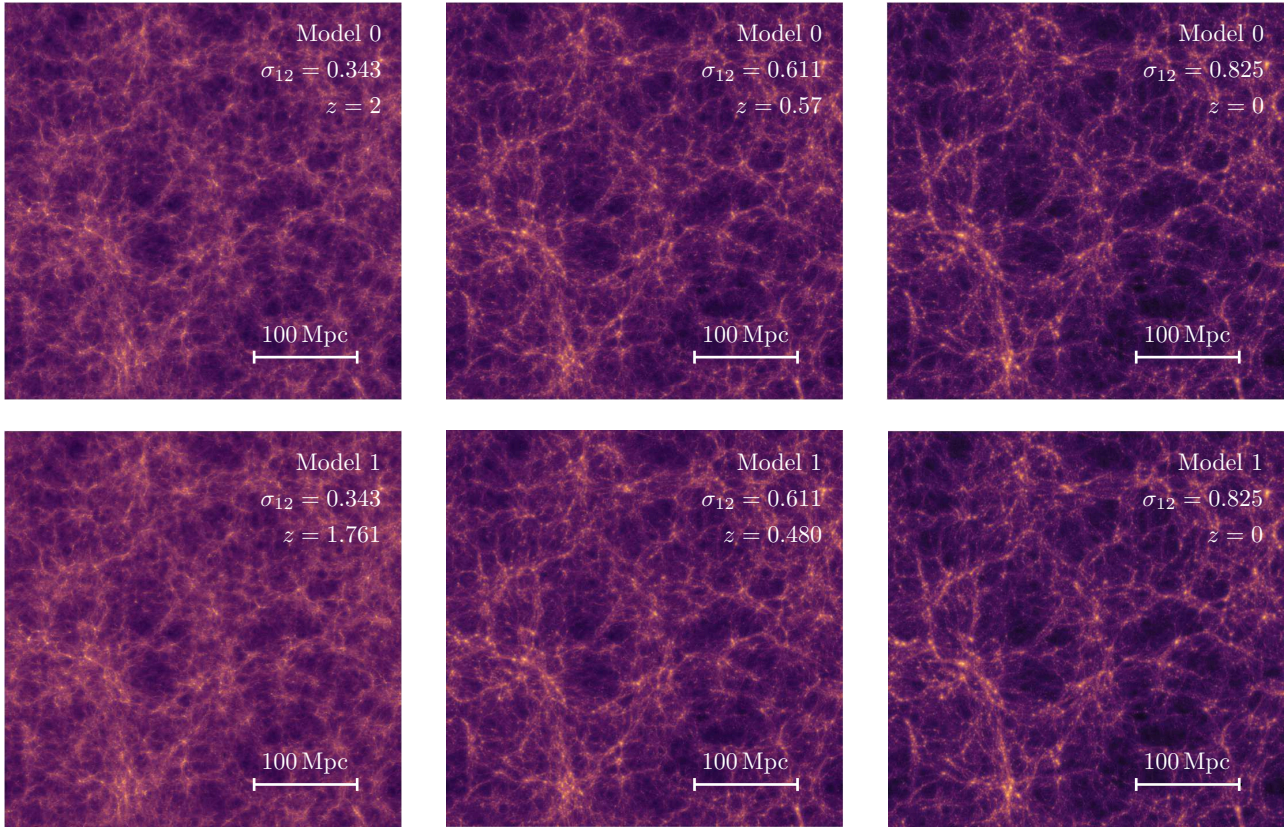
Figure 5. Section of the density field projected over a slice 75 Mpc wide of one of the Aletheia simulations of model 0 (upper panels) and the equivalent one for model 1 (lower panels) at the redshifts corresponding to three of our reference values of σ_{12}. The full pattern of structures such as voids, filaments, and haloes is reproduced with striking agreement in the two realizations. Note that this agreement would be lost if the particle positions were expressed in the commonly used h^{-1}Mpc units as the value of h is different in these two models.

7 but it also gives a good description of the results of all other models, with deviations that remain smaller than 1 per-cent in almost all cases. Despite its simplicity, equation (15) captures the main impact of the different structure formation histories of the Aletheia cosmologies on their respective non-linear power spectra. As we will see in the next section, the same approach can be applied to describe other statistics of the non-linear matter density field.

It is interesting to consider our results in the context of the cosmology rescaling of Angulo & White (2010). For cosmologies with identical linear power spectrum shape, this rescaling reduces to a relabelling of the redshifts to match the global amplitude of density fluctuations as in the relation of equation (13). The additional step of rescaling of the mass – concentration relation of Contreras et al. (2020) is analogous to the correction for the impact of the different structure formation histories in terms of $g(\sigma_{12})$ of equation (15). This picture is consistent with the results of Diemer & Joyce (2019) who found that, although the overall amplitude and shape of $P_L(k|z)$ (characterized by the peak height parameter, $\nu \propto \sigma^{-1}$, and the effective power spectrum slope, $n_{\rm eff}$) can account for most of the cosmology dependence of the concentration – mass relation, a more accurate description requires also information of the growth-rate of cosmic structure in the different models.

3.3 Evolution mapping beyond two-point statistics

The upper panels of Fig. 5 show slices over the box of one of the Aletheia simulations of model 0, at $z = 2, 0.57$, and 0, corresponding to three of our reference values of σ_{12}. The lower panels show slices of the same region of the realization of model 1 with matching initial condition phases, at $z = 1.761, 0.48$, and 0, which correspond to the same values of σ_{12}. These figures illustrate that, when the growth of structure is traced using the global clustering amplitude as a reference, the full density field with its variety of structures is reproduced with striking agreement.

The initial conditions of these simulations differ only in the amplitude of their power spectra. Nusser & Colberg (1998) showed that the equations of motion of a system of collisionless particles can be expressed in a form that is almost independent of the cosmological parameters when the evolution is described in terms of the variable $\tau = \ln D$. Neglecting this weak dependence, the simulations of the two models will follow exactly the same evolution but with a given amplitude of density fluctuations taking place at different values of τ in each case. Using instead the variable $\tau' = \ln \sigma_{12}$, which corresponds to a constant shift in τ for each cosmology, synchronizes both solutions. The weak cosmology dependence of the equations of motion leads to small differences in the two solutions, which become evident in the high-density regions that dominate the power spectrum at high k values.

The similarity illustrated in Fig. 5 suggests that evolution mapping does not only apply to the matter power spectrum. A relation similar to equation (13) must be valid for higher-order N point statistics, geometrical and topological descriptors such as Minkowski functionals, or the full probability distribution function of the density field. We leave a detailed study of such relations for future work. We focus here
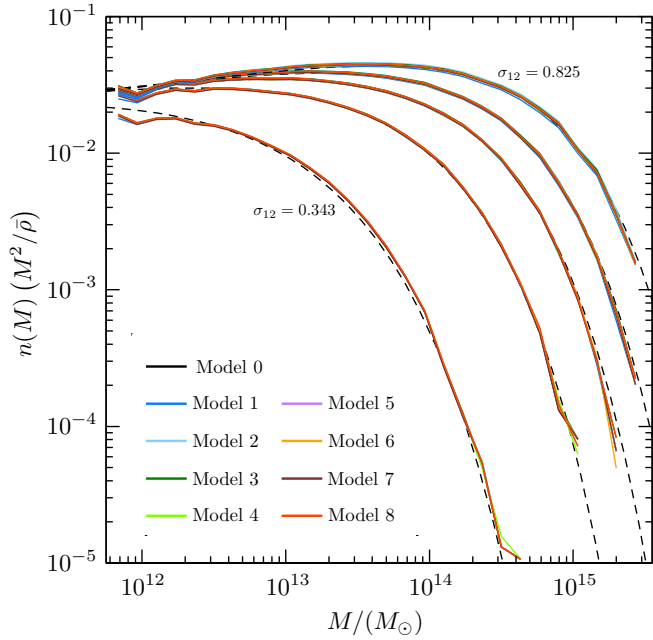
Figure 6. Halo mass functions measured from the Aletheia simulations (solid lines) for the snapshots that correspond to our five reference values of $\sigma_{12}(z)$. The prediction of Tinker et al. (2008) for model 0 (dashed lines) gives a good description of these measurements. The agreement between these measurements is lost when halo masses are expressed in $h^{-1}M_\odot$ units.

on another important source of information of the non-linear matter density field, the halo mass function, $n(M)$.

Most theoretical models of the halo mass function are expressed in terms of the halo multiplicity function given by

$$f(\sigma) = \frac{M}{\bar{\rho}(0)} \frac{dn(M)}{d\ln\left(\sigma^{-1}\right)}, \qquad (16)$$

where $\sigma^2(M)$ represents the variance of the linearly-evolved density field given in equation (7) evaluated at a scale

$$R(M) = \left(\frac{3\,M}{4\pi\bar{\rho}}\right)^{1/3}. \qquad (17)$$

Theoretical recipes based on the spherical or ellipsoidal collapse models predict that $f(\sigma)$ is independent of cosmology and redshift (Press & Schechter 1974; Sheth & Tormen 1999). Using N-body simulations, Jenkins et al. (2001) found that the function $f(\sigma)$ corresponding to different halo definitions is close to universal and provided a fitting function accurate at the 10-20 per-cent level. The same strategy has been followed by several authors (Reed et al. 2003; Warren et al. 2006; Reed et al. 2007; Tinker et al. 2008; Crocce et al. 2010; Watson et al. 2013; Bocquet et al. 2016; Seppi et al. 2020), leading to prescriptions with improved accuracy. In the context of these recipes, cosmologies with identical linear power spectra, and hence equal variance $\sigma^2(M)$, would also have indistinguishable mass functions, implying that a relation analogous to equation (13) should also be valid, at least approximately, for $n(m)$.

To study the applicability of an evolution mapping relation to the mass function, we computed $n(M)$ for the Aletheia simulations. Different definitions of halo mass, M, have been used in the literature primarily based on the friends-of-friends (FOF) percolation algorithm (Davis et al. 1985) or on the spherical overdensity (SO) halo finder (Lacey & Cole 1994), with the latter having a more direct link

to theoretical predictions. SO masses are often defined as a given overdensity with respect to the critical density

$$\rho_{\rm c}(z) = \frac{3\,H(z)^2}{8\pi G}. \qquad (18)$$

However, this definition depends explicitly on the Hubble parameter which, as discussed in Sec. 2, represents a mixture of shape and evolution parameters and would therefore spoil the possible use of an evolution mapping relation for $n(M)$. Instead, we used SO masses defined by the radius enclosing an average density that is a factor $\Delta = 200$ of the mean density of the Universe, $\bar{\rho}(z = 0)$.

We identified dark matter haloes and their properties using ROCK-STAR (Behroozi et al. 2013) and computed the mass functions of all Aletheia simulations averaging the measurements from the pairs corresponding to the same cosmological model. Fig. 6 shows the mass functions of the models for our reference values of σ_{12} plotted as $n(M)(M^2/\bar{\rho}^2(0))$, which are remarkably similar. Note that this agreement would have been hidden for models 1 and 2 if the measurements were expressed in the commonly used units of $h^{-1}M_\odot$ and h^{-1}Mpc as these cosmologies are characterized by different values of h. The black dashed lines show the predictions for the mass function of model 0 at each redshift based on the recipe of Tinker et al. (2008), which is in good agreement with our measurements. The differences between the various models can be seen more clearly in Fig. 7, which shows the ratios of the mass functions of all Aletheia simulations, with respect to that of model 0. These ratios show similar trends as those of $P(k)$, with sub-percent level differences at low values of σ_{12} that increase to a few percent for $\sigma_{12} = 0.825$.

These results indicate that an evolution mapping relation akin to equation (13) for the matter power spectrum is also applicable to $n(M)$, that is

$$n(M|z, \mathbf{\Theta}_{\rm s}, \mathbf{\Theta}_{\rm e}) \simeq n(M|\mathbf{\Theta}_{\rm s}, \sigma_{12}\,(z, \mathbf{\Theta}_{\rm s}, \mathbf{\Theta}_{\rm e})). \qquad (19)$$

In the same way as the non-linear matter power spectrum, the deviations from this relation can be described in terms of the different structure formation histories of these models as

$$
\begin{aligned}
n\left(M|g, g'\right) = {} & n\left(M|g_0\,, g_0'\right) + \frac{\partial n}{\partial g}\left(M|g_0\,, g_0'\right)(g - g_0) \\
& + \frac{\partial n}{\partial g'}\left(M|g_0\,, g_0'\right)\left(g' - g_0'\right),
\end{aligned} \qquad (20)
$$

where we omitted the dependency on $\mathbf{\Theta}_{\rm s}$ and σ_{12}. Fig. 8 shows the ratio between the mass functions of the different Aletheia cosmologies and that inferred using equation (20) with the derivatives with respect to g and g' estimated from the results of models 0, 1, and 7. This relation gives a good description of the mass functions of all models, with the deviations being dominated by the variance of the measurements. As for the case of $P(k)$, the dependence of the residuals from the exact evolution mapping relation for $n(M)$ of equation (19) on the structure formation histories of these cosmologies can be encapsulated into the differences in the values of $g(\sigma_{12})$ and $g'(\sigma_{12})$ at the particular value of σ_{12} being considered.

Several studies have shown that $f(\sigma)$ cannot be described by a universal function at high accuracy as its amplitude and shape are cosmology and redshift dependent (Tinker et al. 2008; Courtin et al. 2011; Despali et al. 2016; Diemer 2020; Ondaro-Mallea et al. 2021). Fig. 9 illustrates this result. The upper panel shows the function $f(\sigma)$ inferred from the Aletheia simulations for our reference values of σ_{12} (solid lines), compared against the $z = 0$ prediction from Tinker et al. (2008), $f_{\rm T}(\sigma|z = 0)$ (dashed lines). The amplitude of the halo multiplicity functions inferred from the simulations decreases with increasing redshift. These deviations can be seen more clearly in
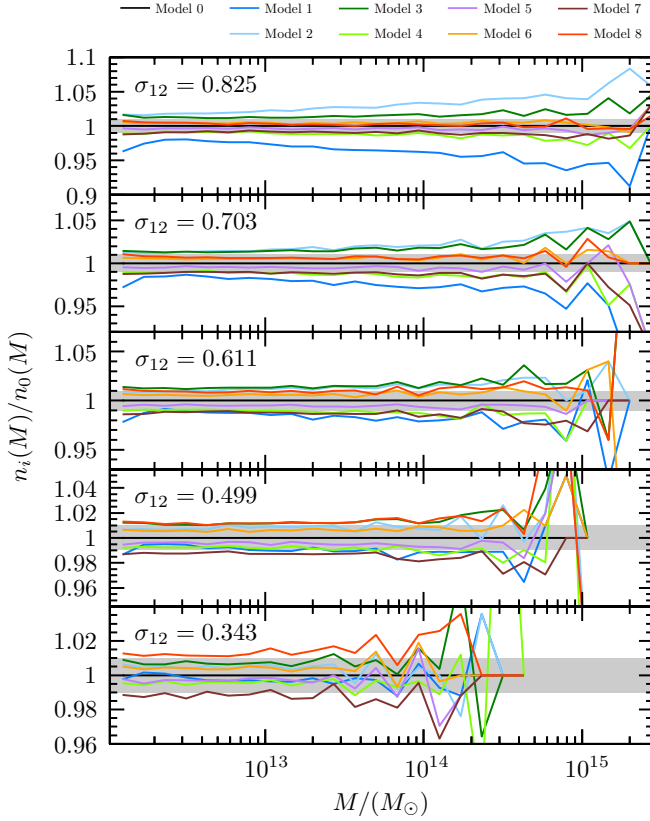
Figure 7. Ratios of the halo mass functions recovered from the different Aletheia simulations and the one corresponding to model 0 for our five reference values of σ_{12}.

Figure 8. Ratios of the halo mass functions recovered from the different models i of the Aletheia simulations and the ones predicted using equation (20) based on the results of model 0 and the differences in the growth suppression factors, Δg_i, and its derivative with respect to σ_{12}, $\Delta g_i'$, for our reference values of σ_{12}.

the lower panel, which shows the ratio of the simulation results with the theory prediction at $z = 0$. This plot also shows that, although they are characterized by different redshifts, the functions $f(\sigma)$ corresponding to a given value of σ_{12} become increasingly similar as this parameter decreases. This suggests that, for this mass definition, the key parameter to describe the deviations from universality of $f(\sigma)$ is σ_{12} and not the redshift explicitly. This can be used to provide improved recipes of the evolution of the mass function that are accurate at high redshifts, specially for cosmologies that deviate from the standard ΛCDM parameters.

4 PRACTICAL APPLICATIONS OF EVOLUTION MAPPING

In this section we focus on the practical applications of the results presented in Sec. 3 on the analysis and interpretation of numerical simulations and cosmological observations.

At the level of the linear evolution of density fluctuations, the deceptively simple relation of equation (13) has several implications as it drastically reduces the number of parameters required to describe $P_L(k|z)$. For example, when using the Markov Chain Monte Carlo (MCMC) technique to derive cosmological parameter constraints from LSS data sets, the values of all evolution parameters such as w_0 or w_a are treated as slow quantities that require a new call to a Boltzmann solver such as CAMB (Lewis et al. 2000) or CLASS (Lesgourgues 2011) to compute $P_L(k|z)$ every time their values are changed. The computational cost of these multiple evaluations is a bottleneck of
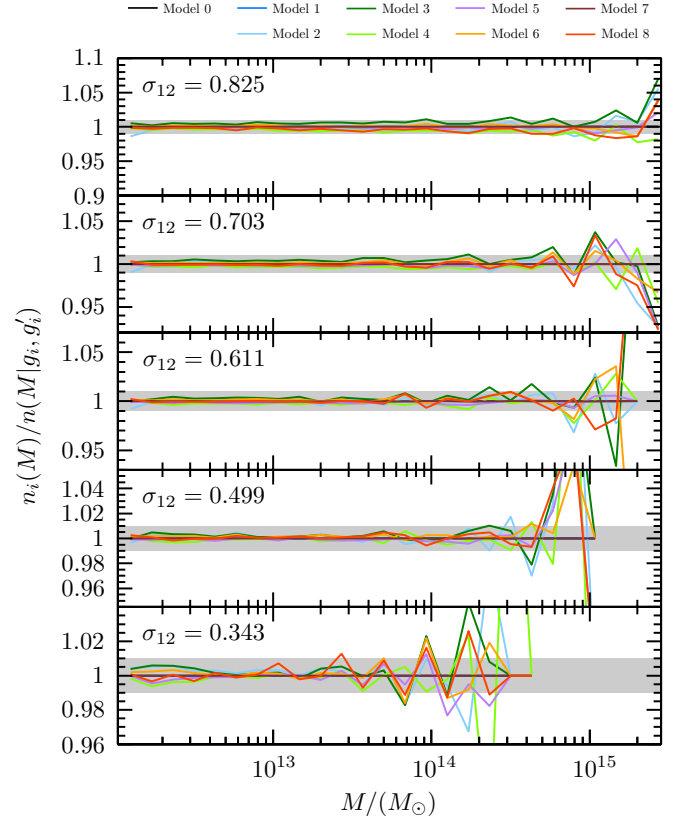
the analysis. However, once the power spectrum of a given model has been computed, a large number of alternative models defined by the same shape parameters and varying evolution parameters can be sampled simply by re-scaling the obtained $P_L(k|z)$, expressed in Mpc units, by the ratios of their corresponding values of $\sigma_{12}^2(z)$. In essence, the only quantities that should be treated as slow parameters are the physical density parameters ω_b, ω_c, and ω_ν that define the shape of the transfer function. This approach can lead to a significant speed-up of current cosmological analyses, allowing us to explore larger parameter spaces in considerably less time.

Recent studies have proposed to reduce the computational cost of parameter inference analyses by means of emulators of $P_L(k|z)$ calibrated on the outputs of Boltzmann solvers (Aricò et al. 2021; Spurio Mancini et al. 2021). These emulators are based on large training sets that sample different cosmological parameters including purely evolution parameters, such as w_0 or w_a, and parameters that represent a mixture of evolution and shape quantities such as $\sigma_{8/h}$ or the fractional density parameters Ω_c and Ω_b. The calibration of these emulators makes use of $P_L(k|z)$ expressed in h^{-1}Mpc units, which is explicitly evaluated at multiple redshifts. A more efficient emulator design can be achieved by exploiting the fact that, when expressed in Mpc units, evolution parameters only affect the linear power spectrum through the value $\sigma_{12}(z)$.

If the dependence of the transfer function, $T(k)$, on the relevant physical density parameters is emulated, it is possible to obtain a prediction for the full power spectrum in Mpc units for any choice
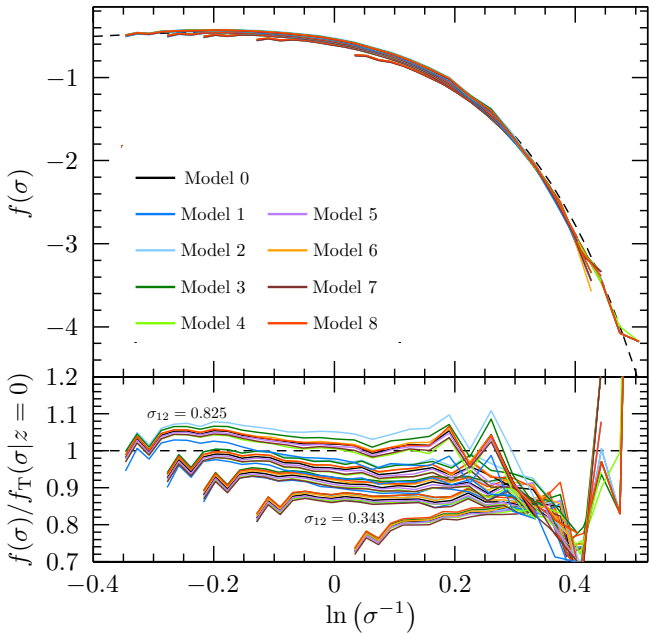
Figure 9. Upper panel: function $f(\sigma)$ defined in equation (16) recovered from the Aletheia simulations for our reference values of σ_{12} (solid lines) compared against the prediction from Tinker et al. (2008) at $z = 0$ (dashed line). Lower panel: ratio between the simulation results and $f_T(\sigma|z = 0)$. The deviations from universality are more correctly described in terms of σ_{12} than the redshift z.

of evolution parameters and redshift. The full shape of $P_L(k|z)$ can be obtained from the output of the emulator of $T(k)$ and n_s (and any additional shape parameter controlling the scale dependence of the primordial power spectrum). The correct amplitude of $P_L(k|z)$ can be obtained by computing the value of $\sigma_{12}(z)$ in terms of the desired normalization at $z = 0$ and the growth factor $D(z)$ for the cosmology being considered. Such recipe would be valid for a wide range of evolution cosmological parameters, including non-standard models such as EDE or other possible dynamic dark dark energy cosmologies, as long as the corresponding linear growth factor is scale independent. The smaller number of parameters required to emulate $T(k)$ should increase the overall accuracy of the predictions, while avoiding the need to sample the redshift evolution of $P_L(k|z)$ explicitly should greatly simplify the calibration procedure.

The evolution mapping relation of equation (13) can also be used to construct more general emulators of the non-linear matter power spectrum. Emulators based on the outputs of N-body simulations have now become a common tool to describe the non-linear evolution of the matter power spectrum (Heitmann et al. 2010, 2016; DeRose et al. 2018; Garrison et al. 2018; Euclid Collaboration et al. 2018, 2020). Due to the high computational cost of the required simulations, the number of nodes in the emulator design must be kept to a minimum. This makes it difficult to explore a high-dimensional cosmological parameter space while maintaining accurate predictions. As a result, current emulators leave out parameters such as the curvature of the Universe, or dynamic dark energy models beyond the standard parametrization of equation (10). A large number of redshift outputs are also required to probe the evolution of these cosmologies, which complicates the calibration of the emulators. These problems could be alleviated by using an alternative emulator design that exploits the mapping between models characterized by the same

value of $\sigma_{12}(z)$. This could be achieved by choosing a reference set of evolution parameters, $\mathbf{\Theta}_{e,0}$, which is kept fixed in all simulations, and sampling only over the parameter space

$$\mathbf{\Phi} = (\mathbf{\Theta}_s, \sigma_{12}). \tag{21}$$

Each node $\mathbf{\Phi}_i = (\mathbf{\Theta}_{s,i}, \sigma_{12,i})$ would correspond to a simulation with the cosmological parameters $(\mathbf{\Theta}_{s,i}, \mathbf{\Theta}_{e,0})$ and a single redshift output such that

$$\sigma_{12}(z, \mathbf{\Theta}_{s,i}, \mathbf{\Theta}_{e,0}) = \sigma_{12,i}. \tag{22}$$

The power spectrum of a cosmology characterized by any set of evolution parameters $\mathbf{\Theta}_e$ could then be obtained by evaluating the emulator at its corresponding value of $\sigma_{12}(z)$. This prediction, which would correspond to the reference set $\mathbf{\Theta}_{e,0}$, could then be transformed to the desired evolution parameters using a recipe similar to equation (15) to account for the different formation histories of the two models. With the exception of this second step, a similar approach was used by Pedersen et al. (2021) to emulate the Lyman-α forest one-dimensional power spectrum in terms of Δ_p^2 (see also McDonald et al. 2005).

The smaller number of parameters involved in the emulation procedure, added to the fact that no explicit sampling of z would be required, would result in more accurate predictions. Furthermore, such an emulator would be automatically valid for all possible choices of evolution parameters. We are currently producing an emulator that will serve as a proof of concept of this design. This emulator, which we call CASSANDRA, will be described in more detail in a forthcoming publication (Gonzalez-Jara et al., in prep.).

The analysis of the halo mass function of Sec. 3.3 suggests that the same general strategy can be applied to model other statistics of the non-linear density field. Using a reference set of evolution parameters, it is possible to study the evolution of the desired statistic as a function of σ_{12}. Those models could then be extended to describe general cosmologies by analysing the impact of the different structure formation histories, characterized by $g(\sigma_{12})$, on the results.

5 CONCLUSIONS

We analysed the impact of different cosmological parameters on the matter power spectrum and on structure formation in general. We classified all parameters into two sets, shape and evolution parameters. The former are parameters that affect the shape of the linear-theory dimensionless power spectrum. The latter include parameters that only determine the time evolution of the amplitude of $\Delta_L^2(k|z)$. The effect of all evolution parameters is degenerate: once the shape parameters are fixed, the linear dimensionless power spectra of models with different evolution parameters that result in the same clustering amplitude, even if this occurs at different redshifts, are identical.

As the linear-theory power spectrum is the key quantity to determine the properties of the non-linear density field, the evolution mapping relation of equation (13) can be used to reduce significantly the number of parameters required to model the impact of non-linearities on $P(k|z)$. We tested this relation using the Aletheia simulations, a set of paired-fixed N-body simulations of nine cosmologies defined by the same shape parameters and a wide array of evolution parameters (summarized in Table 2). When measured at the redshifts for which their respective values of $\sigma_{12}(z)$ are identical, the power spectra of all Aletheia cosmologies are remarkably similar and only show differences of a few percent in the deeply non-linear regime. The residuals with respect to the exact evolution mapping

relation are the result of the different structure formation histories experienced by each model to reach the same value of $\sigma_{12}(z)$. For the range of scales included in this analysis, these differences can be accurately described in terms of the values of $\Delta g(\sigma_{12})$ and $\Delta g'(\sigma_{12})$ between these cosmologies.

The degeneracy between all evolution parameters that lead to the same overall clustering amplitude does not only apply to the matter power spectrum. The full density field inferred from the Aletheia simulations corresponding to the same values of $\sigma_{12}(z)$ are remarkably similar. This suggests that a relation analogous to equation (13) could be valid in general for all statistical descriptions of the density field. As an example, we showed that the halo mass functions of the Aletheia cosmologies are in good agreement, with residuals of a few per cent that can be described in terms of their differences in $g(\sigma_{12})$ and $g'(\sigma_{12})$ using the same general procedure as for $P(k|z)$.

We discussed a few practical applications of the evolution mapping relation. At the linear level, this relation can help to significantly speed up the Bayesian analysis of LSS data sets that require an evaluation of $P_{\mathrm{L}}(k|z)$ for multiple cosmologies by treating all evolution parameters as fast quantities that do not require a new call to a Boltzmann solver. It can also be used to construct general predictions of $P_{\mathrm{L}}(k|z)$ based on an emulator of the dependence of $T(k)$ on the shape parameters. We also proposed a new design for an emulator of the non-linear power spectrum in which only the shape parameters are explicitly sampled and all evolution parameters are implicitly included through different values of σ_{12}. The predictions of this emulator can be adapted to an arbitrary choice of evolution parameters using a recipe similar to equation (15) to account for the different structure formation histories between the reference cosmology and the desired model. Preliminary tests show that an emulator based on this design can provide high accuracy prediction of the non-linear power spectrum for general cosmologies (Gonzalez-Jara et al., in prep.). The same strategy can be applied to other statistics of the density field and can be used as a general approach to describe matter clustering in the non-linear regime.

Although the values of the basic shape parameters are well constrained by present-day CMB observations, our current constraints on evolution parameters still allow for significant deviations from the standard ΛCDM model. It is important to obtain general observational constraints on the evolution of $\sigma_{12}(z)$ as it encapsulates the information on the values of all evolution parameters. Measurements of $\sigma_{12}(z)$ within a particular parameter space also impose strong constraints on the shape of the matter power spectrum in the non-linear regime that can be used to extend current galaxy clustering analyses into smaller scales.

The evolution mapping relations discussed here only become evident when the power spectra and halo mass functions are expressed in Mpc and $M_\odot$ units and cannot be described in terms of the commonly used $\sigma_{8/h}$. Our findings complement the arguments of Sánchez (2020) against the use of the traditional factors of h that are commonly introduced in the units of theoretical predictions for cosmological observables. There is much to be gained by abandoning this practice and expressing models of $P(k|z)$, and the results of cosmological numerical simulations in general, in Mpc units.

DATA AVAILABILITY

The data underlying this article will be shared on reasonable request to the corresponding authors.

REFERENCES

Alam S., et al., 2017, MNRAS, 470, 2617–2652
Alam S., et al., 2021, Phys. Rev. D, 103, 083533
Anderson L., et al., 2012, MNRAS, 427, 3435
Angulo R. E., Pontzen A., 2016, MNRAS, 462, L1
Angulo R. E., White S. D. M., 2010, MNRAS, 405, 143
Angulo R. E., Zennaro M., Contreras S., Aricó G., Pellejero-Ibañez M., Stücker J., 2021, MNRAS,
Aricò G., Angulo R. E., Zennaro M., 2021, arXiv e-prints, p. arXiv:2104.14568
Behroozi P. S., Wechsler R. H., Wu H.-Y., 2013, ApJ, 762, 109
Bird S., Viel M., Haehnelt M. G., 2012, MNRAS, 420, 2551
Bocquet S., Saro A., Dolag K., Mohr J. J., 2016, MNRAS, 456, 2361
Bocquet S., Heitmann K., Habib S., Lawrence E., Uram T., Frontiere N., Pope A., Finkel H., 2020, ApJ, 901, 5
Chevallier M., Polarski D., 2001, International Journal of Modern Physics D, 10, 213
Contreras S., Angulo R. E., Zennaro M., Aricó G., Pellejero-Ibañez M., 2020, MNRAS, 499, 4905
Cooray A., Sheth R., 2002, Physics Reports, 372, 1–129
Courtin J., Rasera Y., Alimi J. M., Corasaniti P. S., Boucher V., Füzfa A., 2011, MNRAS, 410, 1911
Crocce M., Scoccimarro R., 2006, Phys. Rev. D, 73, 063519
Crocce M., Pueblas S., Scoccimarro R., 2006, MNRAS, 373, 369
Crocce M., Fosalba P., Castander F. J., Gaztañaga E., 2010, MNRAS, 403, 1353
DES Collaboration et al., 2021, arXiv e-prints, p. arXiv:2105.13549
DESI Collaboration et al., 2016, arXiv e-prints, p. arXiv:1611.00036
Davis M., Efstathiou G., Frenk C. S., White S. D. M., 1985, ApJ, 292, 371
Dawson K. S., et al., 2013, AJ, 145, 10
Dawson K. S., et al., 2016, AJ, 151, 44
DeRose J., et al., 2018, arXiv e-prints, p. arXiv:1804.05865
Despali G., Giocoli C., Angulo R. E., Tormen G., Sheth R. K., Baso G., Moscardini L., 2016, MNRAS, 456, 2486
Diemer B., 2020, ApJ, 903, 87
Diemer B., Joyce M., 2019, ApJ, 871, 168
Eisenstein D. J., et al., 2005, ApJ, 633, 560
Euclid Collaboration et al., 2018, arXiv e-prints, p. arXiv:1809.04695
Euclid Collaboration et al., 2020, arXiv e-prints, p. arXiv:2010.11288
Garny M., Taule P., 2021, J. Cosmology Astropart. Phys., 2021, 020
Garrison L. H., Eisenstein D. J., Ferrer D., Tinker J. L., Pinto P. A., Weinberg D. H., 2018, The Astrophysical Journal Supplement Series, 236, 43
Grieb J. N., et al., 2017, MNRAS, 467, 2085
Hamilton A. J. S., Kumar P., Lu E., Matthews A., 1991, ApJ, 374, L1
Heitmann K., White M., Wagner C., Habib S., Higdon D., 2010, ApJ, 715, 104

Heitmann K., et al., 2016, ApJ, 820, 108

Heymans C., et al., 2021, A&A, 646, A140

Hikage C., et al., 2019, PASJ, 71, 43

Hildebrandt H., et al., 2018, preprint, p. arXiv:1812.06076 (arXiv:1812.06076)

Ivanov M. M., Simonović M., Zaldarriaga M., 2020, J. Cosmology Astropart. Phys., 2020, 042

Ivezić Ž., et al., 2019, ApJ, 873, 111

Jain B., Mo H. J., White S. D. M., 1995, MNRAS, 276, L25

Jenkins A., Frenk C. S., White S. D. M., Colberg J. M., Cole S., Evrard A. E., Couchman H. M. P., Yoshida N., 2001, MNRAS, 321, 372

Kaiser N., 1987, MNRAS, 227, 1

Lacey C., Cole S., 1994, MNRAS, 271, 676

Laureijs R., et al., 2011, arXiv e-prints, p. arXiv:1110.3193

Lesgourgues J., 2011, arXiv e-prints, p. arXiv:1104.2932

Lewis A., Challinor A., Lasenby A., 2000, ApJ, 538, 473

Linder E. V., 2003, Physical Review Letters, 90, 091301

Ma Z., 2007, ApJ, 665, 887

Ma C.-P., Fry J. N., 2000, ApJ, 543, 503

McClintock T., et al., 2019, ApJ, 872, 53

McDonald P., et al., 2005, ApJ, 635, 761

McDonald P., Trac H., Contaldi C., 2006, MNRAS, 366, 547

Mead A. J., 2017, MNRAS, 464, 1282

Mead A. J., Peacock J. A., Heymans C., Joudaki S., Heavens A. F., 2015, MNRAS, 454, 1958

Mead A. J., Heymans C., Lombriser L., Peacock J. A., Steele O. I., Winther H. A., 2016, MNRAS, 459, 1468

Mead A. J., Brieden S., Tröster T., Heymans C., 2021, MNRAS, 502, 1401

Nishimichi T., Bernardeau F., Taruya A., 2017, Phys. Rev. D, 96, 123515

Nusser A., Colberg J. M., 1998, MNRAS, 294, 457

Ondaro-Mallea L., Angulo R. E., Zennaro M., Contreras S., Aricò G., 2021, arXiv e-prints, p. arXiv:2102.08958

Peacock J. A., Dodds S. J., 1994, MNRAS, 267, 1020

Peacock J. A., Dodds S. J., 1996, MNRAS, 280, L19

Pedersen C., Font-Ribera A., Rogers K. K., McDonald P., Peiris H. V., Pontzen A., Slosar A., 2021, J. Cosmology Astropart. Phys., 2021, 033

Perlmutter S., et al., 1999, ApJ, 517, 565

Planck Collaboration et al., 2020, A&A, 641, A6

Press W. H., Schechter P., 1974, ApJ, 187, 425

Reed D., Gardner J., Quinn T., Stadel J., Fardal M., Lake G., Governato F., 2003, MNRAS, 346, 565

Reed D. S., Bower R., Frenk C. S., Jenkins A., Theuns T., 2007, MNRAS, 374, 2

Riess A. G., et al., 1998, AJ, 116, 1009

Sánchez A. G., 2020, Phys. Rev. D, 102, 123511

Sánchez A. G., et al., 2017, MNRAS, 464, 1493–1501

Scoccimarro R., Colombi S., Fry J. N., Frieman J. A., Hivon E., Melott A., 1998, ApJ, 496, 586

Seljak U., 2000, MNRAS, 318, 203

Seppi R., et al., 2020, arXiv e-prints, p. arXiv:2008.03179

Sheth R. K., Tormen G., 1999, MNRAS, 308, 119

Smith R. E., et al., 2003, MNRAS, 341, 1311

Spergel D., et al., 2015, arXiv e-prints, p. arXiv:1503.03757

Springel V., Pakmor R., Zier O., Reinecke M., 2021, MNRAS, 506, 2871

Spurio Mancini A., Piras D., Alsing J., Joachimi B., Hobson M. P., 2021, arXiv e-prints, p. arXiv:2106.03846

Takahashi R., 2008, Progress of Theoretical Physics, 120, 549

Takahashi R., Sato M., Nishimichi T., Taruya A., Oguri M., 2012, ApJ, 761, 152

Taruya A., 2016, Phys. Rev. D, 94, 023504

Taruya A., Bernardeau F., Nishimichi T., Codis S., 2012, Phys. Rev. D, 86, 103528

Tinker J., Kravtsov A. V., Klypin A., Abazajian K., Warren M., Yepes G., Gottlöber S., Holz D. E., 2008, ApJ, 688, 709

Tröster T., et al., 2020, A&A, 633, L10

Troxel M. A., et al., 2018, Phys. Rev. D, 98, 043528

Warren M. S., Abazajian K., Holz D. E., Teodoro L., 2006, ApJ, 646, 881

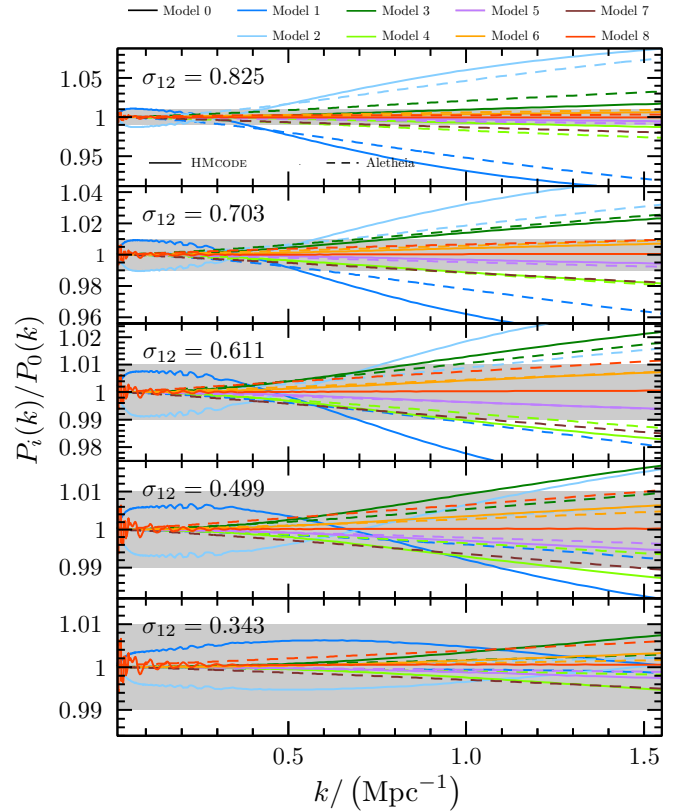**Figure A1.** Ratios of the power spectra of the test cosmologies defined in Table 2 with that of model 0 for our reference values of σ_{12} as predicted by HMCODE (solid lines). For comparison, the dashed lines show the results obtained from the Aletheia simulations (matching those shown in Fig. 3).

Watson W. A., Iliev I. T., D'Aloisio A., Knebe A., Shapiro P. R., Yepes G., 2013, MNRAS, 433, 1230

Wetterich C., 2004, Physics Letters B, 594, 17

d'Amico G., Gleyzes J., Kokron N., Markovic K., Senatore L., Zhang P., Beutler F., Gil-Marín H., 2020, J. Cosmology Astropart. Phys., 2020, 005

APPENDIX A: COMPARISON WITH AVAILABLE PREDICTION SCHEMES OF THE NON-LINEAR POWER SPECTRUM

In this section, we test the ability of current recipes of the non-linear $P(k|z)$ to reproduce the relation between models with identical values of $\sigma_{12}(z)$ described in Section 3.2. We focus on two such recipes, namely, (i) the HMCODE prescription (Mead et al. 2015, 2016, 2021) as implemented in CAMB, and (ii) on the EUCLIDEMULATOR 2 (Euclid Collaboration et al. 2020). As these recipes have not been designed to account for the evolution-mapping relation of equation (13), it is interesting to test how well they can reproduce the ratios of the power spectra of the different Aletheia simulations.

The recipe of HMCODE is based on the halo model of structure formation (Ma & Fry 2000; Seljak 2000; Cooray & Sheth 2002) and produces power spectra predictions that are accurate at the 5 per cent level for a wide range of non-standard cosmologies. The solid lines in Fig. A1 show the predictions obtained with HMCODE of the ratios of the power spectra of all Aletheia cosmologies with that of model 0 for our reference values of σ_{12}. For comparison, the results
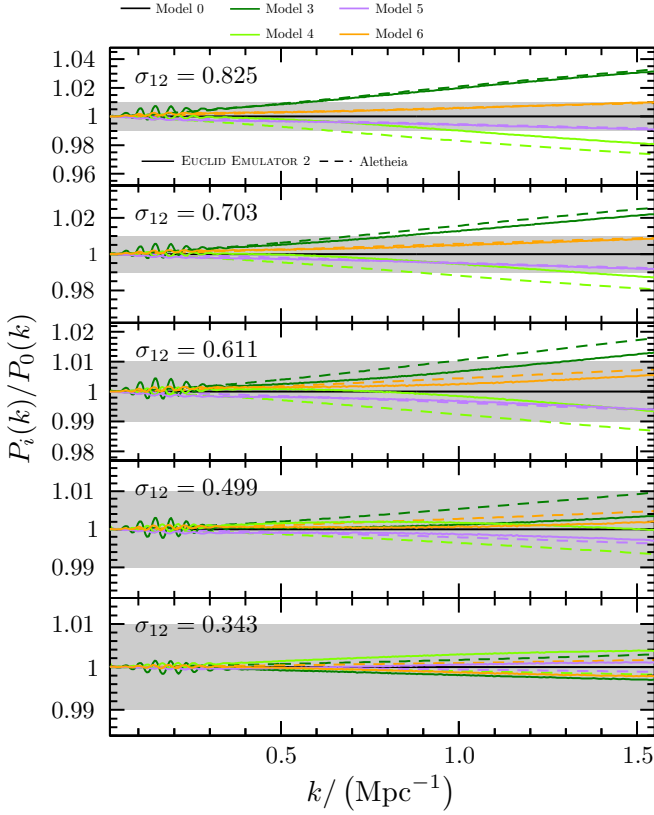
Figure A2. Same as Fig. A1 but based on the predictions of the EUCLIDEMU-LATOR 2 (solid lines). Only the models that fall within the allowed parameter ranges of the emulator are included. The dashed lines show the results of the corresponding Aletheia simulations (also shown in Fig. 3).

inferred from the Aletheia simulations are shown by the dashed lines. In general, HMCODE gives an adequate description of the results of the simulations, with differences at the level of a few per cent within the range of scales considered here.

Rather than emulating $P(k|z)$ directly, the EUCLIDEMULATOR 2 predicts the boost factor, $B(k)$, defined as the ratio

$$B(k|z) = \frac{P(k|z)}{P_L(k|z)}. \tag{A1}$$

As for each reference value of σ_{12} the linear-theory power spectra of our test cosmologies are identical, the ratio of the boost factors predicted by the emulator corresponds to the ratio of $P(k|z)$. Of all the cosmologies defined in Table 2, only models 0 and 3 – 6 fall within the parameter ranges of the EUCLIDEMULATOR 2. The solid lines in Fig. A2 show the ratios of the power spectra of these cosmologies with that of model 0 as predicted by the emulator. The dashed lines show the results obtained from the Aletheia simulations. The emulator gives an accurate description of the simulation results, with sub-percent level deviations in all cases. This agreement suggests that a relation similar to equation (15) could help to extend the applicability of the emulator outside its current parameter range.

This paper has been typeset from a TEX/LATEX file prepared by the author.